



HAL
open science

Extraction of non-continuous orbital frequencies from noisy insolation data and from palaeoproxy records of geomagnetic intensity using the phase of continuous wavelet transforms

Ginette Saracco, Nicolas Thouveny, Didier Boulès, Julien Carcaillet

► To cite this version:

Ginette Saracco, Nicolas Thouveny, Didier Boulès, Julien Carcaillet. Extraction of non-continuous orbital frequencies from noisy insolation data and from palaeoproxy records of geomagnetic intensity using the phase of continuous wavelet transforms. *Geophysical Journal International*, 2009, 176 (3), pp.767-781. 10.1111/j.1365-246X.2008.04057.x . hal-03099092

HAL Id: hal-03099092

<https://hal.science/hal-03099092>

Submitted on 6 Jan 2021

HAL is a multi-disciplinary open access archive for the deposit and dissemination of scientific research documents, whether they are published or not. The documents may come from teaching and research institutions in France or abroad, or from public or private research centers.

L'archive ouverte pluridisciplinaire **HAL**, est destinée au dépôt et à la diffusion de documents scientifiques de niveau recherche, publiés ou non, émanant des établissements d'enseignement et de recherche français ou étrangers, des laboratoires publics ou privés.

Extraction of non-continuous orbital frequencies from noisy insolation data and from palaeoproxy records of geomagnetic intensity using the phase of continuous wavelet transforms

Ginette Saracco,¹ Nicolas Thouveny,¹ Didier L. Boulès¹ and Julien T. Carcaillet^{1,2}

¹CNRS-UMR 6635, CEREGE, UPCAM, Géophysique & Planétologie, Europole de l'Arbois, BP 80, 13545 Aix en Provence, France.

E-mail: saracco@cerege.fr

²CNRS-UMR 5025, LGCA, 1381 Rue Piscine, BP 53, 38041 Grenoble, France

Accepted 2008 December 3. Received 2008 December 2; in original form 2008 May 19

SUMMARY

The presence or absence of orbital frequencies in the palaeomagnetic field spectrum is the subject of intense discussions. While palaeoclimatic variations, i.e. glacial/interglacial alternation periods, are known to be governed by insolation variations via orbital frequencies, the link between such frequencies and the geomagnetic field maintenance processes (convection and rotation in the fluid metallic core) remains unclear. The study of frequency behaviour of long time-series proxy records requires a robust and linear time-frequency method with local and scale analysis properties. For these reasons, we use algorithms based on complex continuous wavelet theory and the stationary phase method, first developed in acoustics in the years 1988–1991, for extracting frequency and amplitude modulation laws of arbitrary signals from the phase of their wavelet transform. This method is robust in the presence of noise and does not require restrictive conditions on the energy of signals.

After introducing the basis of the method with some illustrations on periodic signals, we show the efficiency of our algorithms on a synthetic insolation signal (Milankovitch cycles), by extracting the main three orbital frequencies (precession, obliquity and eccentricity); then we show its robustness in the presence of a high level of noise. Finally, we apply this method to various proxy records of (i) past climate variations ($\delta^{18}\text{O}$), (ii) the past geomagnetic field intensity variations recorded by ocean sediments and (iii) along the deep-seafloor basalts and (iv) variations of the production of cosmogenic nuclide ($^{10}\text{Be}/^9\text{Be}$). Our results confirm the presence of orbital frequencies in all these palaeoproxy records and suggest an orbital forcing of geomagnetic field variations via geodynamo processes.

Key words: Time series analysis; Wavelet transform; Earth rotation variations; Geomagnetic excursions; Palaeointensity.

1 INTRODUCTION

Since the Earth's magnetic field was supposed to be generated by convection of conducting fluids in the outer core (dynamo action), several authors (e.g. Poincaré 1910; Malkus 1968) have envisaged that it could be maintained or influenced by the Earth's axis precessional motion. After several decades of debate, independent lines of evidence demonstrate that this hypothesis cannot be rejected: (i) the power required to drive the geodynamo might be supplied by axis precession (e.g. Vanyo 1991; Vanyo & Dunn 2001; Christensen & Tilgner 2004; Wu & Roberts 2008); (ii) the precession of a spherical container filled with conducting fluid produces a period of motion identical to the period of rotation and induces a varying magnetic field, able to reverse its polarity (e.g. Tilgner 2005). Spectral analyses of palaeointensity and palaeoinclination

records have often revealed significant variation at Earth's orbital frequencies.

The fact that sedimentary palaeomagnetic records of long term variations of the field intensity and directions contain significant variance at orbital frequencies led authors to conclude either that orbital motion influenced the geodynamo (e.g. Yokoyama & Yamazaki 2000; Yamazaki & Oda 2002) or that palaeomagnetic records are contaminated by orbitally driven palaeoenvironmental signals (e.g. Kent 1982; Channell *et al.* 1998; Guyodo *et al.* 2000; Xuan & Channell 2008).

These latter interpretations do not take into account other major arguments: (i) over the last Myr, the polarity changed mostly at time of low amplitude obliquity variation (Fuller 2006); (ii) proxy records of the geomagnetic field variation at the last Myr scale are produced from non-palaeomagnetic methods such as

cosmogenic nuclide records $^{10}\text{Be}/^9\text{Be}$ (e.g. Carcaillet *et al.* 2003, 2004b) and deep-seafloor magnetization record (e.g. Gee *et al.* 2000). These provide independent observations supporting a preferential occurrence of dipole lows and excursions during or at the end of interglacial episodes (Thouveny *et al.* 2004), and a possible link with obliquity variations (see Thouveny *et al.* 2008, for a complete review).

Finally neither the theory, the numerical and experimental developments, nor analysis of palaeodata series allows rejection of the hypothesis of an orbital forcing of the geodynamo, but one must recognize that astronomical periods are most often poorly resolved by classical methods of spectral analysis and sometimes poorly understood.

These spectral analyses are limited because they do not allow an accurate estimation of spectral components and their time evolution as time-frequency or time-scale methods. Recent studies based on time-scale investigation with complex wavelets (Berger *et al.* 1998; Guyodo *et al.* 2000; Heslop 2007) use only the modulus of the wavelet transform, while only the phase allows us to extract the instantaneous frequencies of signals.

In the present paper, we describe a method based on the phase of complex continuous wavelet transform (CCWT) for extracting instantaneous frequencies adapted to long time-series such as insolation and palaeoproxy records.

The first methods for extracting frequencies and amplitude modulation laws were developed in the area of acoustics (Kronland-Martinet 1989; Saracco 1989; Saracco *et al.* 1990a,b, 1991; Guillemain *et al.* 1991; Delprat *et al.* 1991; Valero & Saracco 2005). The interest of these methods, based on the phase of the CCWT, is that they can be applied to regions where the modulus of the transform is small. Here, we show that the method can be applied to a large class of signals with respect to the analysing wavelet. Some extensions of these methods (Kronland-Martinet 1989; Saracco 1989; Saracco *et al.* 1990b, 1991; Guillemain *et al.* 1991) were successfully used with the Gabor transform (Delprat *et al.* 1991; Guillemain & Kronland-Martinet 1996; Carmona *et al.* 1999). This classical time-frequency transform (Gabor 1946) is also linear, but the analysing window is translated in time and translated in frequency domain, while the analysing wavelet (time-scale transform) is translated in time and dilated in time to cover the time-frequency space. This dilation property gives a local and multi-scale analysis of transient phenomena that classical time-frequency methods do not allow. If the analysing wavelet is complex, the wavelet transform will be complex and we obtain two complementary informations, the phase and the modulus of the analysed signal.

From the phase we show the possibility to extract a set of ridges or spectral lines corresponding to frequency modulation laws of arbitrary signals with respect to the analysing wavelet, while the values of modulus along these ridges provide amplitude modulation laws. The bases of this method are introduced in Section 2 and some illustrations with periodic signals are shown. We then apply this method to a synthetic insolation signal (Milankovitch cycles over 5 Myr BP), Section 3. The main three orbital frequencies (precession, obliquity and eccentricity) are extracted and analysed. They correspond to complex beat phenomena, but they are usually assimilated to the mean values of, respectively, 19.5 or 23 kyr, 41 kyr and the two modes of eccentricity 100 and 400 kyr. A zoom around the eccentricity component is made, and the robustness of the method in the presence of a high level of noise (white Gaussian noise) is shown. We then apply, Section 4, our algorithm to various palaeoproxy records (palaeoclimate proxy, $\delta^{18}\text{O}$, cosmogenic nuclide iso-

topes and magnetic palaeointensity). Results and interpretations are discussed in Section 5.

2 BACKGROUND AND DEFINITIONS: EXTRACTION OF FREQUENCY AND AMPLITUDE MODULATION LAWS

2.1 High-frequency asymptotic approximation

Using a high-frequency approximation, known as the saddle-point method, Debye's development (Erdélyi 1956; Copson 1967), we can estimate integrals of the following form:

$$\int_{\Gamma} A(\mu) \exp(i\beta p(\mu)) d\mu, \quad (1)$$

where Γ represents a path in the complex plane. A and p are regular analytic functions of the complex variable μ , and β is a parameter with real part tending to infinity.

For large values of $|\beta|$, the main contribution of integral (1) comes from points μ_0 , where the derivative of p vanishes, called cols or saddle points (complex plane) or stationary phase points (real axis). At these points, and for large values of $|\beta|$, the exponential function is maximal. Along the lines of steepest descent: $\text{Im}[\beta p(\mu)] = C^{\text{ste}}$, the exponential decays quickly and the phase is constant. The integration path is limited to the neighbourhood of saddle points (Γ').

If $\mu \in \mathcal{C}$, $p(\mu)$ verifies:

$$\text{Im}[p(\mu)] = \text{Im}[p(\mu_0)] = C^{\text{ste}}. \quad (2)$$

$\text{Re}[p(\mu_0)]$ is maximal on Γ'

$$\left. \frac{dp(\mu)}{d\mu} \right|_{\mu = \mu_0} = 0, \quad \text{for } \mu = \mu_0, \quad (3)$$

where:

$$\frac{dp(\mu)}{d\mu} = \frac{\partial \text{Re}[p(\mu)]}{\partial x} - i \frac{\partial \text{Re}[p(\mu)]}{\partial y}, \quad (\text{Cauchy conditions}).$$

If p is a function of the real variable μ , the main contribution of the integral (1) comes from points of stationary phase μ_0 which cancel $p'(\mu)$. The integral (oscillating integral) is then limited to neighbourhoods of stationary points. For stationary points of order one [i.e. when only the first derivative vanishes, $p'(\mu_0) = 0$ and $p''(\mu_0) \neq 0$] the error of the approximation is of order $o(\beta^{-1})$. For stationary points of order n [i.e. if $p'(\mu_0) = \dots = p^{(n)}(\mu_0) = 0$ and $p^{(n+1)}(\mu_0) \neq 0$], the result is valid to order $o(\beta^{-1/n})$ (Erdélyi 1956; Copson 1967; Saracco 1989).

2.2 Complex wavelet transform

Let $x(t)$ be the real-valued square-integrable signal to be analysed. As is customary, we associate to x the complex-valued function $s(t) = x(t) + i(\mathcal{H}x)(t)$, the 'analytic signal' associated to x , where \mathcal{H} represents the Hilbert transform (Papoulis 1984). We shall write $A_x(t) = |s(t)|$ and $\Phi_x(t) = \arg(s(t))$, so that the complex-valued $s(t)$ is:

$$s(t) = A_x(t) \exp(i\Phi_x(t)).$$

The 'instantaneous frequency' of $s(t)$ at time t is defined as

$$v(t) = \frac{1}{2\pi} \frac{d\Phi_x(t)}{dt}. \quad (4)$$

For any analytic signal, $v(t) \geq 0$ for all t . This fact will be used below.

Let $g(t)$ be the complex analysing wavelet of amplitude $A_g(t)$ and phase $\Phi_g(t)$. $g(t)$ has to satisfy a – not very restrictive – admissibility condition:

$$\int \frac{|\hat{g}(\omega)|^2}{|\omega|} d\omega = C_g < \infty, \quad (5)$$

where \hat{g} is the Fourier transform of g . In practice, this means $\hat{g}(0) = 0$, that is, g is of zero mean or $\int g(t) dt = 0$.

This condition is deduced from the requirement of isometry of the transform; it allows us to interpret the square modulus of wavelet coefficients as a density of energy in the time-scale half-plane. Moreover g is chosen to be progressive [i.e. $\hat{g}(\omega) = 0$, for $\omega < 0$]. The progressivity is a necessary condition to eliminate interferences due to spectral components on the negative axis (Saracco 1989, 1994; Valero & Saracco 2005).

The continuous wavelet transform of an arbitrary signal $s(t)$ is defined as the scalar product of the signal and the translated (T^b) and dilated (D^a) analysing wavelet $g[(t-b)/a]$ in the time-scale half-plane (b, a) , $b \in \mathcal{R}$, $a > 0$. The translation parameter b has the dimension of time while the scale or dilation parameter is dimensionless and plays the role of a zoom in frequency domain. Small dilations are related to high frequencies, and large dilations to low frequencies:

$$\begin{aligned} L(b, a) &= \langle T^b D^a g | s \rangle \\ &= a^{-\alpha} \int s(t) \bar{g}\left(\frac{t-b}{a}\right) dt, \\ L(b, a) &= a^{-\alpha} \int A_x(t) A_{\bar{g}}\left(\frac{t-b}{a}\right) \\ &\quad \times \exp i \left(\Phi_x(t) - \Phi_{\bar{g}}\left(\frac{t-b}{a}\right) \right) dt. \end{aligned} \quad (6)$$

\bar{g} is the complex conjugate of g , α the normalization coefficient ($\alpha = 1$, with L^1 normalization, and $\alpha = 1/2$ with L^2 normalization).

The admissibility condition guarantees that the scalar product $\langle s_1, s_2 \rangle$ of any two signals is equal to the scalar product

$$\frac{1}{C_g} \int L(b, a) \bar{L}(b, a) \frac{da db}{a^2} \quad (7)$$

of their wavelet transforms. If a function $F(b, a)$ is the wavelet transform of a signal with respect to a given admissible wavelet g , then F must satisfy the reproducing equation

$$F(b, a) = \iint \mathcal{N}(b, a, b', a') F(b', a') \frac{da db}{a^2}, \quad (8)$$

where $\mathcal{N}(b, a, b', a') = \langle T^b D^a g, T^{b'} D^{a'} g \rangle$ is known as the reproducing kernel. This equation shows that the values of a function which is a wavelet transform are strongly correlated; this means that there is a redundancy of information. Consequently, it is natural to look for subsets of points in the time-scale half-plane which carry ‘relevant information’. The intuitive way is to define trajectories or spectral lines (ridges), representative of frequency modulation laws of the signal along which the energy is concentrated (Kronland-Martinet 1989; Saracco 1989; Saracco *et al.* 1990a (trajectories with respect to dilation parameters); Saracco *et al.* 1990b, 1991; Guillemin *et al.* 1991 (trajectories with respect to translation parameters). From the reproducing equation and the restriction of the wavelet transform along ridges, we can rebuilt the signal or some contributions of the signal (Valero & Saracco 2005). The developments that follow gives one way to construct such subsets.

2.3 Wavelet transform in the asymptotic regime

By eq. (6) above, the phase of any wavelet transform taken for a fixed value of a is

$$\Phi_x(t) - \Phi_g\left(\frac{t-b}{a}\right). \quad (9)$$

Differentiating the above equation, we see that the phase is stationary at points $t_i(a)$ for which

$$v(t_i) = \frac{d}{dt} \Phi_g\left(\frac{t_i-b}{a}\right). \quad (10)$$

Varying a , we obtain a set of spectral lines or multiridges [trajectories of stationary phase points $t_i(a) = \tau(a)$] representing the instantaneous frequencies $\nu_a(t_i(a))$ of the signal in the time-scale half-plane, with respect to the analysing wavelet g .

Let be Ψ_L the argument of the complex continuous wavelet transform, and \mathcal{M} its modulus. The set of stationary phase points defining a set of ridges is obtained for $\frac{d\Psi_L(t)}{dt} = 0|_{\tau(a)}$. It follows, for stationary points of order one (Saracco 1989; Saracco *et al.* 1990b), that

$$\begin{aligned} L(b, a) &= C^{st} \sqrt{\frac{2\pi}{a|A_x''(\tau(a))|}} A_x(\tau(a)) A_g(t\omega) \\ &\quad \times \exp i \left(\Phi_x(\tau(a)) + \Phi_g((\tau(a) - b)/a) \right) \\ &\quad \times \exp \left(i \frac{\pi \operatorname{sgn}[\Phi_x''(\tau(a))]}{4} \right) + o(\beta^{-1}(a)). \end{aligned} \quad (11)$$

If we consider a second-order limited expansion of the phase of the integrand (6), we obtain a Gaussian integral where the modulus \mathcal{M} and the phase Ψ of the transform can be obtained analytically if the analysing wavelet has a Gaussian amplitude and verifies some properties (Saracco 1989; Saracco *et al.* 1990b; Valero & Saracco 2005).

Here, the best choice of analysing wavelet is a wavelet of Morlet type (modulated Gaussian), since (i) its phase $\Phi_{\bar{g}} = \omega_0$ is linear in time for every a , (ii) its modulus is a Gaussian function, (iii) it is (practically) progressive ($\omega_0 \geq 5.5$) and (iv) an appropriate choice of the parameter ω_0 introduces arbitrarily rapid oscillations in the integrals to be evaluated.

$\mathcal{M}(\tau(a), a)$ is locally maximal along ridges

$$\frac{d\Psi(b, a)}{db} = \frac{\omega_0}{a} \quad \text{at } b = \tau(a). \quad (12)$$

It should be emphasized that several maxima of the modulus in general exist in the half-plane (b, a) , which are not stationary points for the phase.

The wavelet coefficients along the set of ridges depend linearly on the analytic signal $s(t)$

$$L(\tau(a), a) - C_1 s(t) = C_2.$$

The set of ridges defined from stationary phase points verifies (12) and gives an estimation of the frequency modulation laws, instantaneous frequencies of the signal (see Figs 1–3). The restriction of the modulus of wavelet transform along ridges gives an estimation of the amplitude modulation laws. Note that we never need to calculate the full wavelet transform of the signal, to find frequency and amplitude modulation laws, since they are directly calculated from the search of stationary phase points of the CCWT phase, in the time-scale half-plane. This method is robust in the presence of a high level of noise, Gaussian white noise (see Section 3; Valero

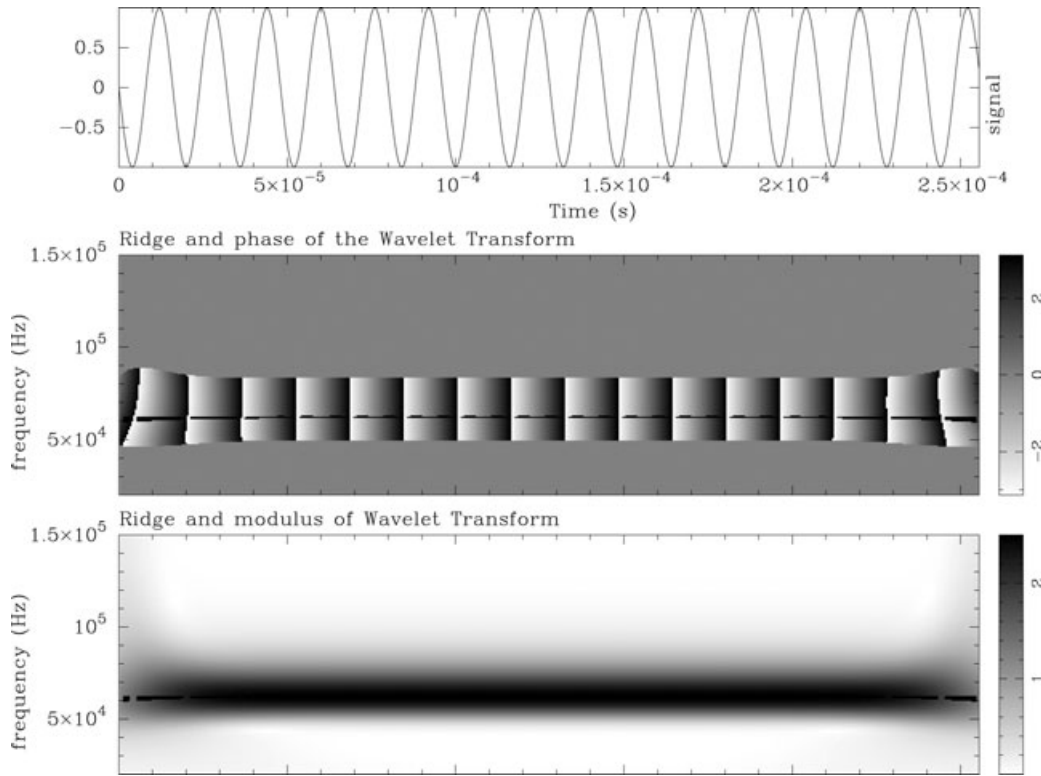


Figure 1. Top: monochromatic signal. Sinusoid of 62.5 kHz frequency. Middle: phase of the CCWT of the sinusoid. The phase is displayed from 0 to 2π . The superimposed horizontal black line extracted from the phase represents exactly the frequency 62.5 kHz of the sinusoid. Bottom: modulus of the CCWT of the monochromatic signal. The modulus is represented in density of points, where black is the maxima and white is zero.

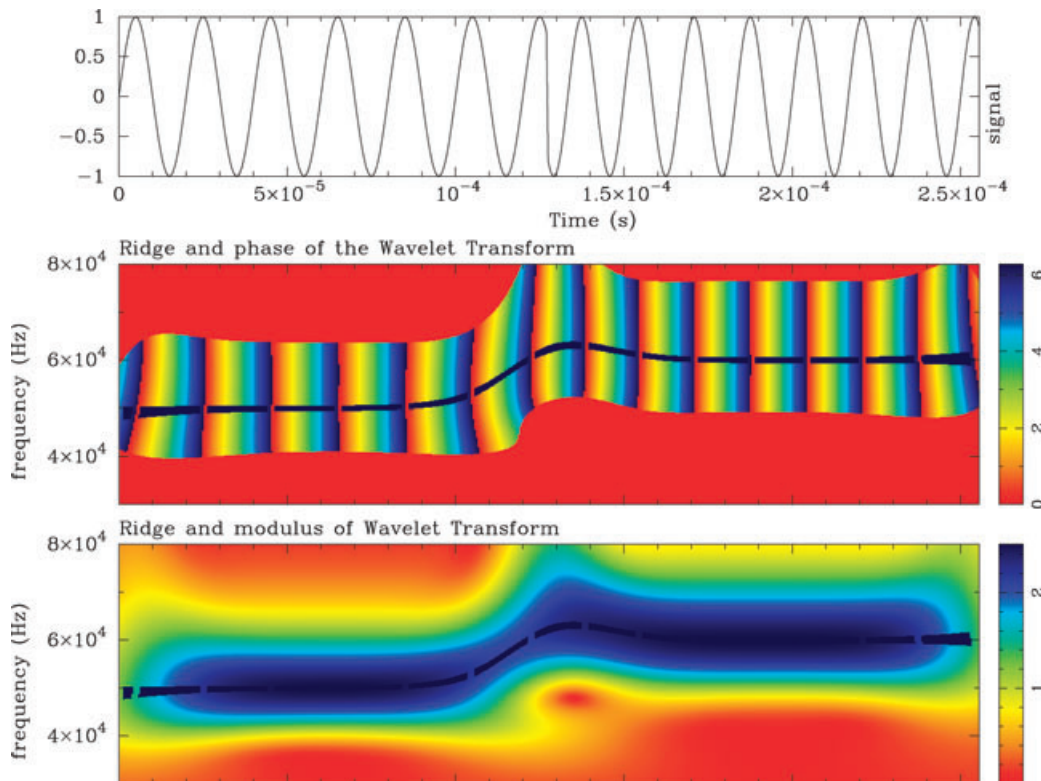


Figure 2. Top: transition between two monochromatic signals. Sinusoids of frequency 50 and 60 kHz. Middle: phase of the CCWT of the signal. The superimposed black line extracted from the phase represents the frequency modulation law of the signal and indicates the frequency of each sinusoid and their transition. Bottom: modulus of the CCWT of the signal. The phase is represented between 0 and 2π . The modulus is displayed in colour codes where the maximum of energy is blue and the minimum is red.

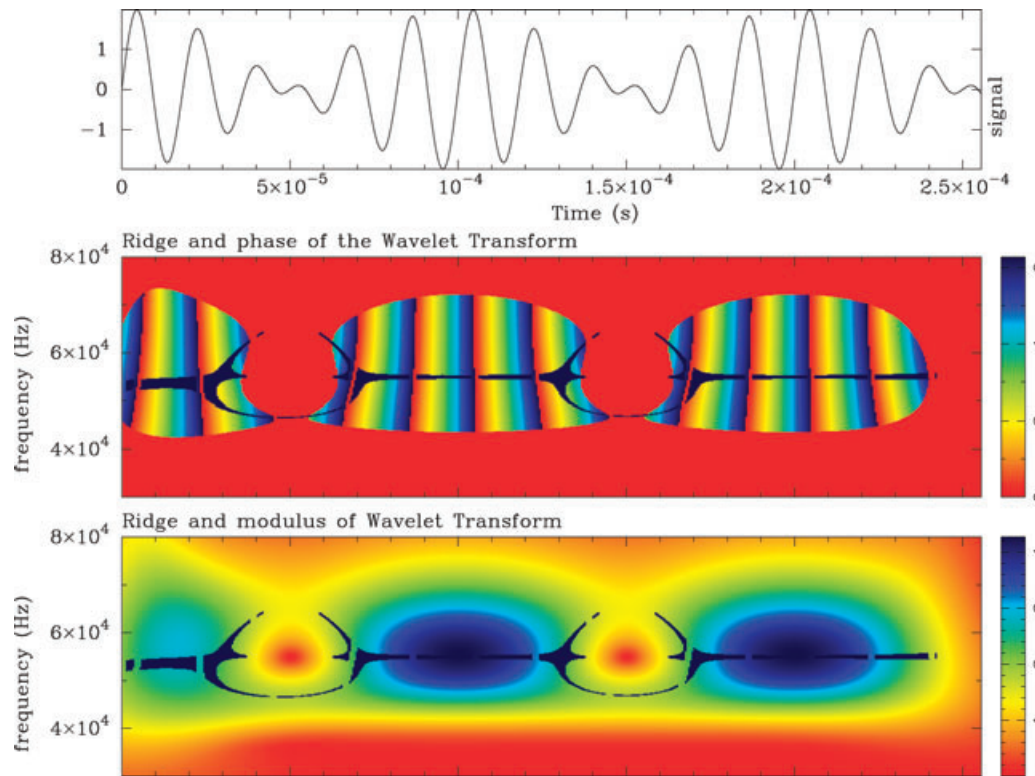


Figure 3. Top: sum of two sinusoids of 50 and 60 kHz. A beat phenomenon appears. Middle: phase of the CCWT of the summation. The superimposed black line (ridge) shows the beat phenomena between the two sinusoids (loop and envelope frequency of 55 kHz). Bottom: modulus of the CCWT of the summation.

& Saracco 2005). For multiridge detection on highly noisy signal, a useful algorithm is the one based on a form of Markov chain Monte Carlo technique (Carmona *et al.* 1999 or Moreau *et al.* 1996).

As a help to understanding of the method, we applied our algorithm successively (1) on a monochromatic signal, a sinusoid of 62.5 kHz (Fig. 1), (2) a transition of two sinusoids of frequency 50 and 60 kHz (Fig. 2) and (3) the sum of two close monochromatic signals (Fig. 3). Time-scale analyses are obtained with a complex analysing wavelet of Morlet type (modulated Gaussian function, with $\omega_0 = 2\pi$). The progressivity property of the wavelet is verified.

All figures display from top to bottom: (1) the time evolution of signal; (2) the phase of the complex continuous wavelet transform and (3) the modulus. We emphasize the fact that the colour codes expressing the modulus are opposed to the usual codes: that is, blue represents the maximum of energy and red the minimum. The phase is represented from zero to 2π . In Fig. 1, the modulus and phase are displayed in density of points, where black colour represents the maximum and white the minimum. The sets of ridges are calculated and extracted from the phase of the CCWT, location of the set of stationary phase points. They are represented by superimposed black lines on the phase and drawn also on the modulus. Cut-offs on the phase limit the expression of ridges. The first cut-off is chosen regarding to the extrema of wavelet coefficients, a second cut-off defines the width of ridges.

Since the wavelet transform is of zero mean value, when the dilated analysing wavelet oscillates at the same pulsation of the sinusoid, the modulus of the CCWT reaches its maximum value. The modulus will be constant and maximum as long as the sinusoid will persist. The phase oscillates with the same frequency as the signal. A simple calculation gives the expression $L(b, a) =$

$(1/2)a^{1/2}\bar{g}(a\omega_0)\exp(ib\omega_0)$. The ridge extracted (horizontal black line) represents the exact value (62.5 kHz) of the frequency component of the sinusoid (Fig. 1). We find (Fig. 2) the two frequency components 50 and 60 kHz (two horizontal black ridges at different times). A local analysis of the change between the two sinusoids shows a convergence of lines of constant phase through the time $t_0 = 1.25 \cdot 10^{-4}$ s, where the transition occurs (analysis of an isolated discontinuity, Grossmann *et al.* 1987; Saracco 1989; Saracco *et al.* 2004, 2007). A sum of two sinusoids (Fig. 3) generates a beat phenomenon in the time-scale half-plane due to the constructive and destructive interferences of two close spectral components. We recognize the envelope frequency $[(\omega_1 + \omega_2)/2 = 55 \text{ kHz}]$ of the signal, and a characteristic loop centred around destructive interferences (minima of energy).

3 APPLICATION TO INSOLATION SIGNAL: EXTRACTION OF PRECESSION, OBLIQUITY AND ECCENTRICITY

The link between palaeoclimate and orbital parameters (equinoctial precession, obliquity and eccentricity) with a complete astronomical theory of the Pleistocene ice ages was principally developed by Milankovitch in 1941. It was since verified that insolation variation is the controlling factor of the successive glacial/interglacial cycles of the Plio-Pleistocene (Berger 1988; Berger & Loutre 1991, 2004; Laskar *et al.* 1993; Berger *et al.* 2005). The astronomical parameters of the Earth's orbit and rotation were obtained (Berger & Loutre 1991) from a numerical solution of a Lagrangian system of nine planetary point masses motion around the Sun, and from an analytical solution of Poisson equations of the Earth–Moon system. We

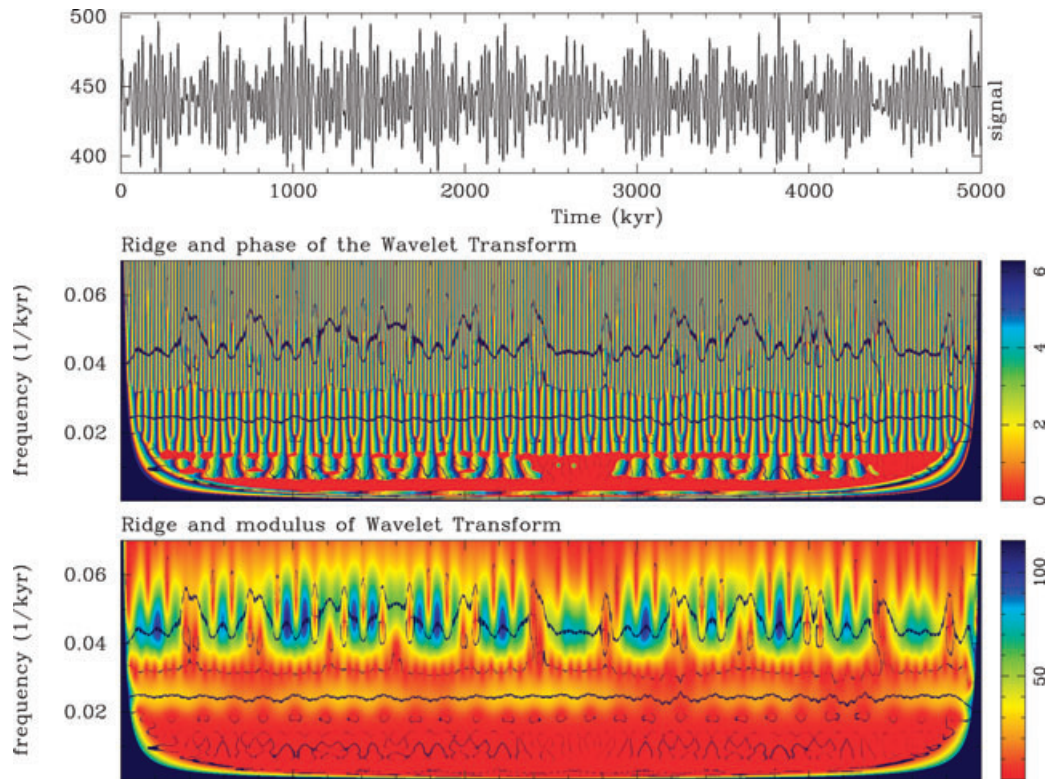


Figure 4. Top: insolation signal of 65°N (July) during 5 Myr. Middle: phase of the CCWT of the insolation signal: the superimposed black lines are the ridges of orbital frequencies (precession, [0.042–0.058] (kyr)⁻¹, obliquity, [0.025–0.026] (kyr)⁻¹ and eccentricity (two lines), [0.008–0.012] and [0.0025] (kyr)⁻¹) extracted from the phase. Bottom: modulus of the CCWT of the insolation signal.

have applied a continuous wavelet transform to the insolation signal over a 5 Myr duration (65°N, July insolation in W m^{-2}) (Berger & Loutre 1991) where a multiridge extraction of orbital components is made. The analysing wavelet is of a Morlet type ($\omega_0 = 2\pi$, see Section 2).

The superimposed black lines represent the different ridges calculated from the phase of the CCWT, trajectories of stationary phase points along the time axis (Fig. 4). The set of ridges associated to orbital parameters are like complex beat phenomena (see Fig. 3), resulting from pseudo-periodic deformation of the Earth's orbit and from pseudo-periodic motions of the Earth's rotation axis.

A pure monochromatic frequency provides a straight and horizontal black line (ridge; see Fig. 1). At the other extreme, a vertical ridge corresponds to the presence of all frequencies, and characterizes an impulse function or Dirac's distribution.

There appear four oscillations characterizing equinoctial precession, obliquity and the two modes of eccentricity (Fig. 4). Ridges calculated from the phase of the CCWT of insolation are also drawn on the modulus. These instantaneous frequencies extracted over 5 Myr belong to frequency ranges: [0.042–0.058], [0.025–0.026], [0.008–0.012] (kyr)⁻¹ and [0.0025] (kyr)⁻¹, respectively, for precession, obliquity and eccentricity (two modes).

This means periods of [17.24–25.64] kyr for precession, [38.4–46.5] kyr for obliquity and [83–125] and [400] kyr, for the two modes of eccentricity. The edge effects (≈ 10 per cent) due to abrupt change at the end and at the beginning of signals, which increase with the dilation parameter 'a', are not represented on the phase and the modulus (Figs 4–7). These edge effects are analogous, in the time-scale half-plane, to the wavelet transform of a Delta's distribution (see edge effects Fig. 8).

The results show (Fig. 4) that the four orbital components (instantaneous frequencies) of the insolation signal cannot be reduced to pure frequencies of 19.5 or 23 kyr, 41, 100 and/or 400 kyr, with constant and strong energy, contrarily to accepted opinion. It is usual for the sake of simplification to take a mean value of components rather than the components themselves. This comes from classic spectral analysis where time-frequency information is not considered.

The respective contributions of precession, obliquity and eccentricity used to compute the insolation signal vary with the chosen date and latitude. If some variations or instabilities occur, the estimates of instantaneous frequencies change but the frequency ranges remain almost the same.

To show the efficiency of our method based on the phase of the CCWT, we compare results of multiridges (frequency modulation laws) extracted from the insolation signal (Figs 4 and 5), and from pure astronomical parameters (Milankovitch cycles; Berger & Loutre 1991) for the eccentricity (Figs 6 and 7), the obliquity (Fig. 8) and the precession (Fig. 9).

The weak energy around the eccentricity component does not allow to prove its effective contribution without information on the phase, as one can see in Fig. 4. We present in Fig. 5 a zoom of the insolation signal around the frequency range of eccentricity ([0.005–0.015] (kyr)⁻¹), and in Fig. 6 the instantaneous frequency calculated from the pure eccentricity component (astronomical parameter) in the same range. At this scale, 15 per cent of the wavelet transform is removed to cancel the edge effects. Although the modulus of eccentricity is weak compared to precession and obliquity components, the calculation of ridges from the phase of the CCWT is still possible.

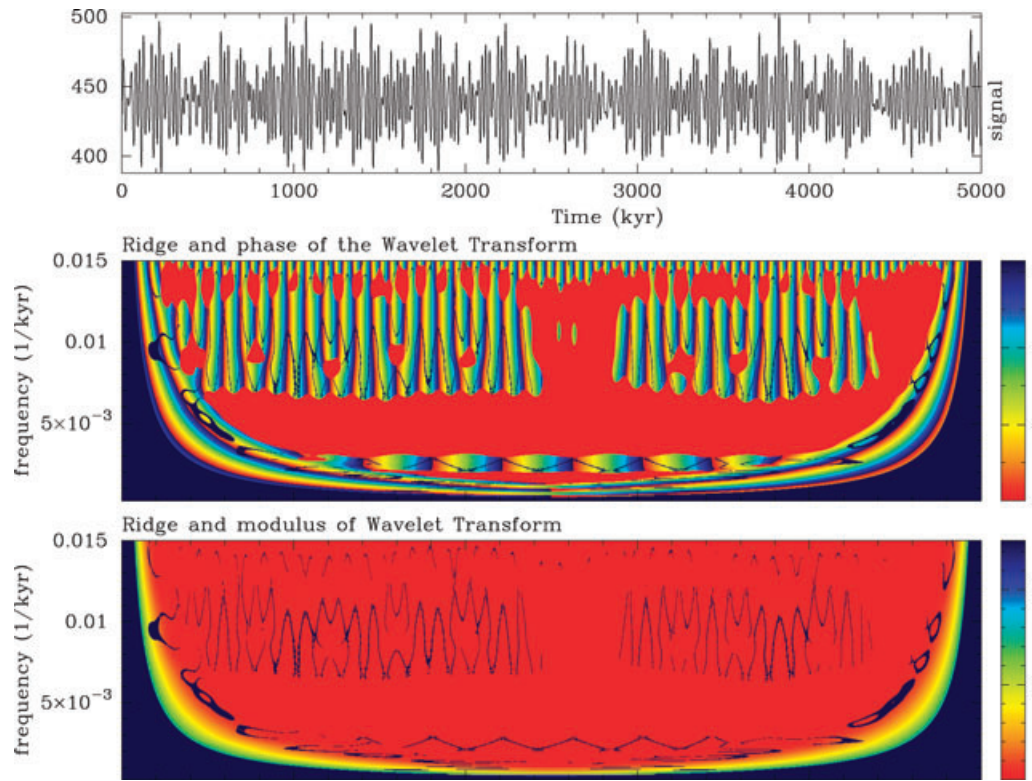


Figure 5. Top: insolation signal of 65°N (July) during 5 Myr as Fig. 4. Zoom in the frequency range of $[0.015-2.5 \cdot 10^{-4}] \text{ (kyr)}^{-1}$. Analysis of the eccentricity component. Middle: phase of the CCWT of eccentricity component. Extraction of the two eccentricity ridges (≈ 102 and ≈ 400 kyr although the modulus is weak compared to precession and obliquity components of the insolation signal (see Fig. 4). Bottom: modulus of the CCWT of eccentricity (weak energy).

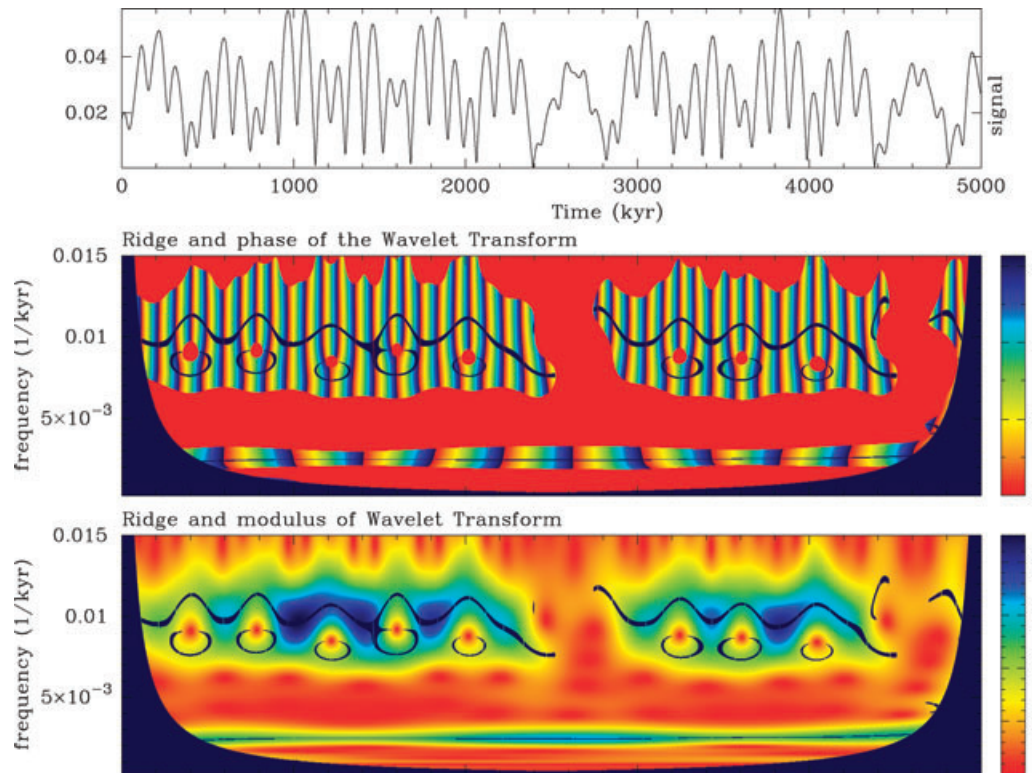


Figure 6. Top: eccentricity component. Middle: Phase of the CCWT of eccentricity component: The two superimposed lines are the ridges of eccentricity frequencies $[0.008-0.012] \text{ (kyr)}^{-1}$ and $0.0025 \text{ (kyr)}^{-1}$ (i.e. [83–125] kyr, 400 kyr) extracted from the phase. Bottom: Modulus of the CCWT of eccentricity component.

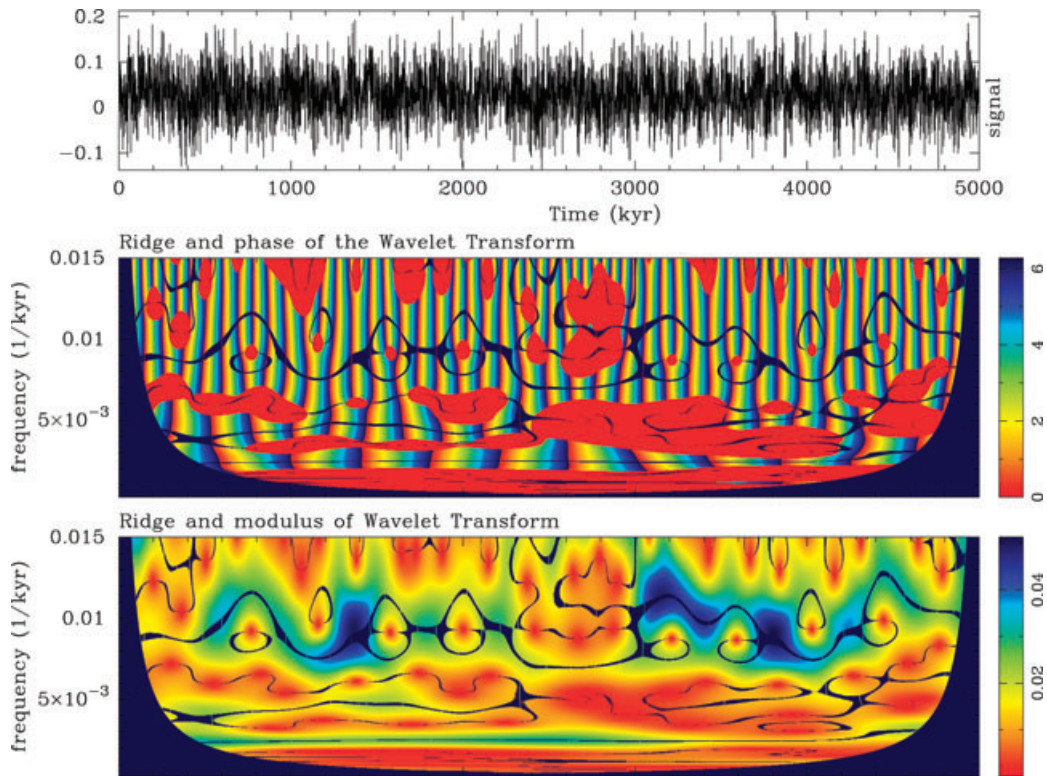


Figure 7. Top: eccentricity component (see Fig. 6) in presence of a white Gaussian noise with a signal/noise ratio of 0.5. Middle: phase of the CCWT of eccentricity. Spectrum is enriched by the noise. However, the two ridges extracted from the phase give a good estimation of orbital eccentricity (≈ 102 and ≈ 400 ka). Bottom: modulus of the CCWT of eccentricity.

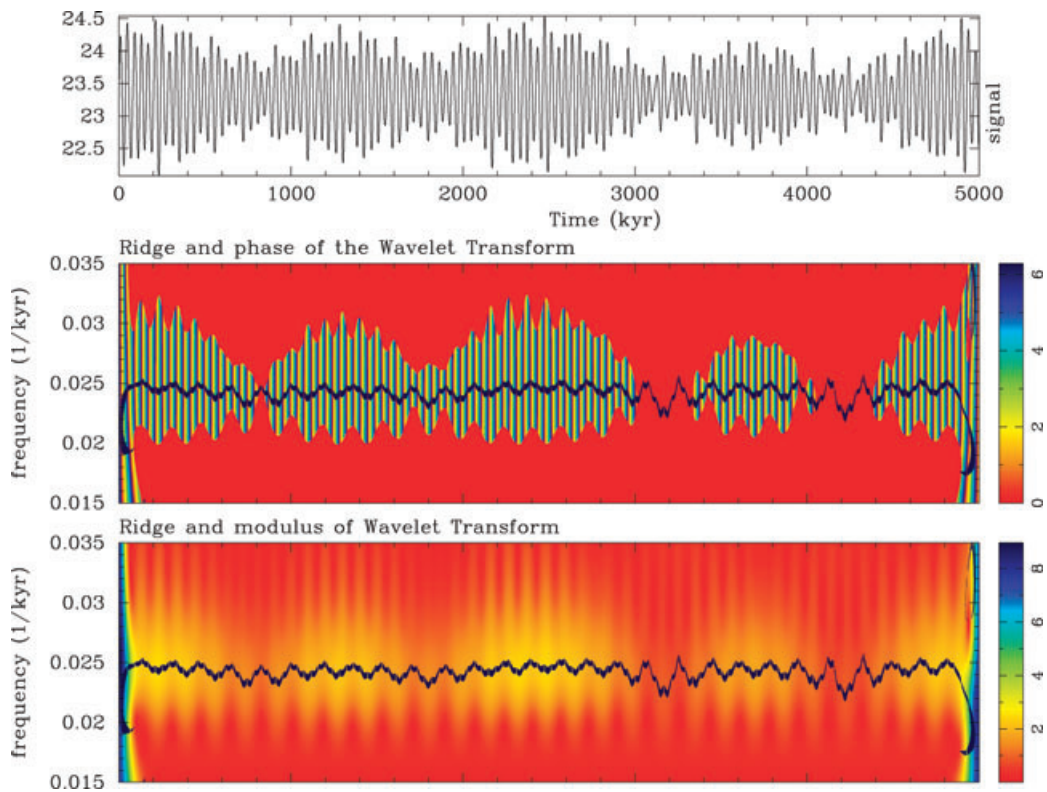


Figure 8. Top: obliquity component. Middle: phase of the CCWT of the obliquity. The superimposed black line represents the instantaneous frequency of obliquity with oscillations between $[0.023$ and $0.026]$ $(\text{kyr})^{-1}$ (i.e. $[38.5$ – $43.4]$ kyr). The vertical ridges are due to the abrupt cut of signal (extremities) (these ridges are similar to the ridge of a Delta's distribution). Bottom: modulus of the CCWT of obliquity.

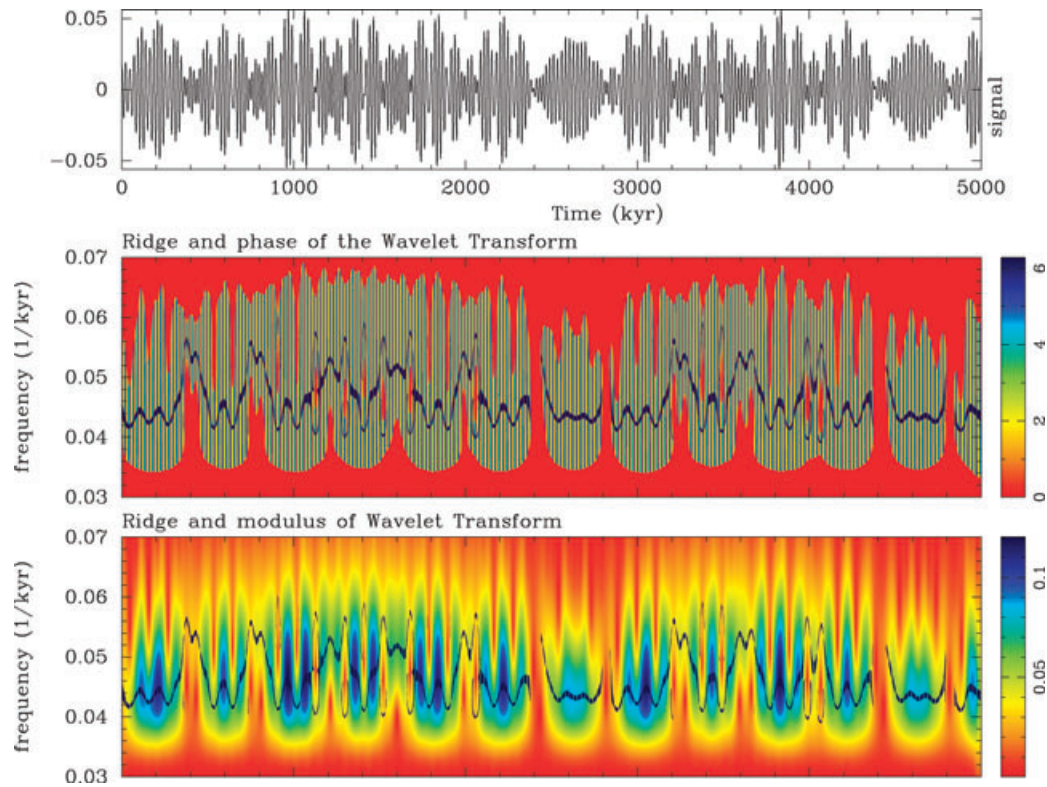


Figure 9. Top: precession component. Middle: phase of the CCWT of the precession. The superimposed black line represents the instantaneous frequency of precession between $[0.042 \text{ and } 0.058] \text{ (kyr)}^{-1}$ (i.e. 17 and 24 kyr). Bottom: modulus of the CCWT of precession.

The high-frequency ridge of eccentricity (first mode), extracted from the phase of insolation (Fig. 5), oscillates faster than the ridge extracted from the phase of the pure eccentricity (Fig. 6), but these oscillations are centred around $0.0098 \text{ (kyr)}^{-1}$ ($T = 102 \text{ kyr}$) and are contained in the frequency range $[0.012\text{--}0.007] \text{ (kyr)}^{-1}$ similarly to the eccentricity component (astronomical parameter). The second ridge approximate period around 400 kyr is quasi the same in both figures.

No model of noise for insolation or proxy records is known. To show the robustness of our method in the presence of a highly noise such a white Gaussian noise, we have oversaturated the original eccentricity component, with a signal-over-noise ratio of 0.5 (Fig. 7). Local secondary ridges due to the noise are added to the pure eccentricity ridge. Despite this noise artificially introduced and the resulting enrichment of the spectrum, a correct estimation of frequency modulations laws is still possible.

The absence of ‘loop’ in the ridge of the obliquity component (Fig. 8) shows that this ‘periodic’ component is not due to the sum of periodic cosinusoids with a beat phenomenon, as Fig. 3. This ridge oscillates around the frequency of 0.024 (kyr)^{-1} ($T = 41.66 \text{ kyr}$) during the last 3 Myr, and around $0.0235 \text{ (kyr)}^{-1}$ ($T = 42.55 \text{ kyr}$) the first 2 Myr. The obliquity is itself modulated by a high-frequency component (Complementary studies on amplitude and frequency variations of the Earth’s obliquity can be found in the paper of Melice *et al.* (2001)). The two vertical ridges observed at the ends of the signal (characteristic of a Delta’s distribution) are due to the abrupt cut of the signal. Compared to the obliquity ridge calculated from insolation signal (Fig. 4), the results are almost the same.

Fig. 9 shows the complexity of the frequency modulation laws of the equinoctial precession component, as we have already found in Fig. 4 (precession ridge extracted from the insolation data). There is

no constant energy during the time, or around a particular frequency, and the ridge oscillates in the interval $[0.041\text{--}0.059] \text{ (kyr)}^{-1}$ ($T = [16.94\text{--}24.39] \text{ kyr}$) including the two frequencies of 19.5 and 23 kyr and not the pseudo period of 26 kyr (Earth’s rotation axis), as Berger (1977) showed. The ridge extracted (Fig. 9) is similar to the ridge extracted from insolation signal (Fig. 4).

The extraction of multiridges from insolation data, corresponding to instantaneous frequencies of orbital components, allows a better understanding of the time evolution of the shape of the Earth’s orbit, the motions of its rotation axis and the spectrum of orbital parameters. This method can be extended to the study of palaeoproxy records without an ‘*a priori*’ hypothesis of possible orbital contributions or influences in the past geomagnetic field or geodynamo process.

4 APPLICATIONS TO PROXY RECORDS OF PALAEOCLIMATIC AND PALAEOGEOLOGICAL VARIATIONS

We have analysed various proxy records of the past climate and past geomagnetic field with the multiridges extraction algorithm described in Section 2. The first application deals with a palaeoclimatic proxy record, which is supposed to be directly influenced by orbital frequencies via insolation variations: the $\delta^{18}\text{O}$ record of core MD900963 (Indian Ocean; Bassinot *et al.* 1994) (Fig. 10). The second series of applications deals with the past geomagnetic field activity records (Figs 11–15).

The use of information carried by the phase of the CCWT allows us to calculate instantaneous frequencies of palaeoproxy records. We discuss here only ridges corresponding to orbital frequencies.

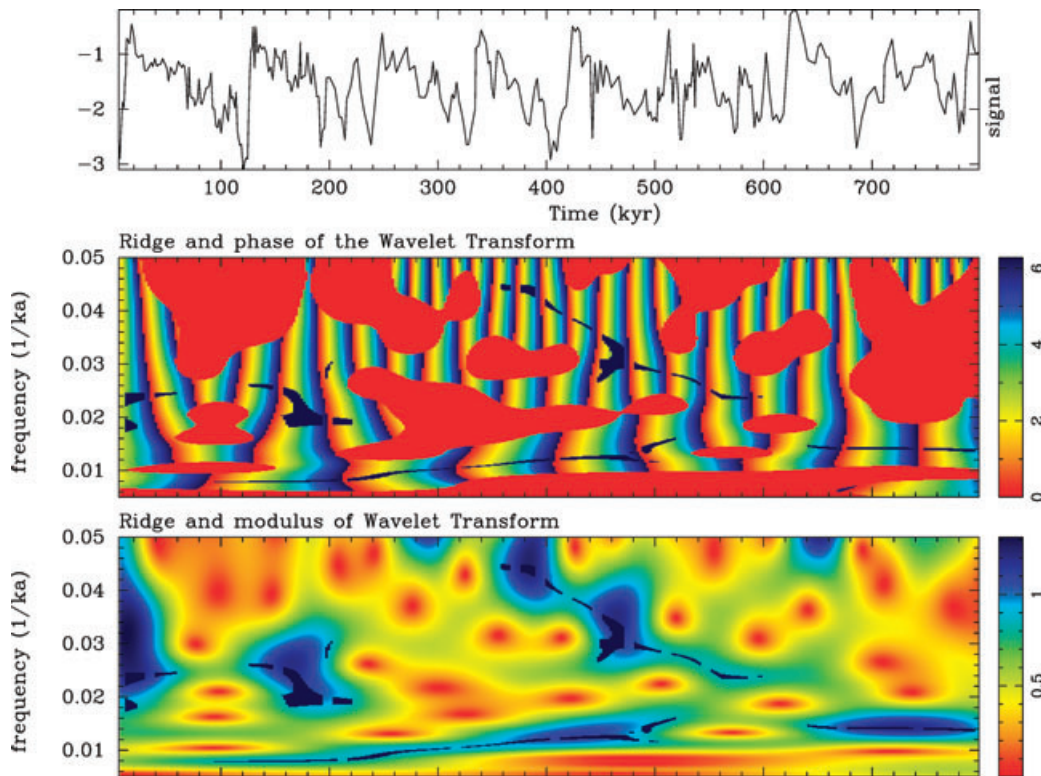


Figure 10. Top: proxy record of the past climate: benthic $\delta^{18}O$ of MD900963 (Maldive area) over the last 800 kyr. Middle: phase of the CCWT with orbital frequencies extracted (superimposed black lines): continuous ridge for eccentricity and discontinuous ridge for obliquity. Bottom: modulus of the CCWT .

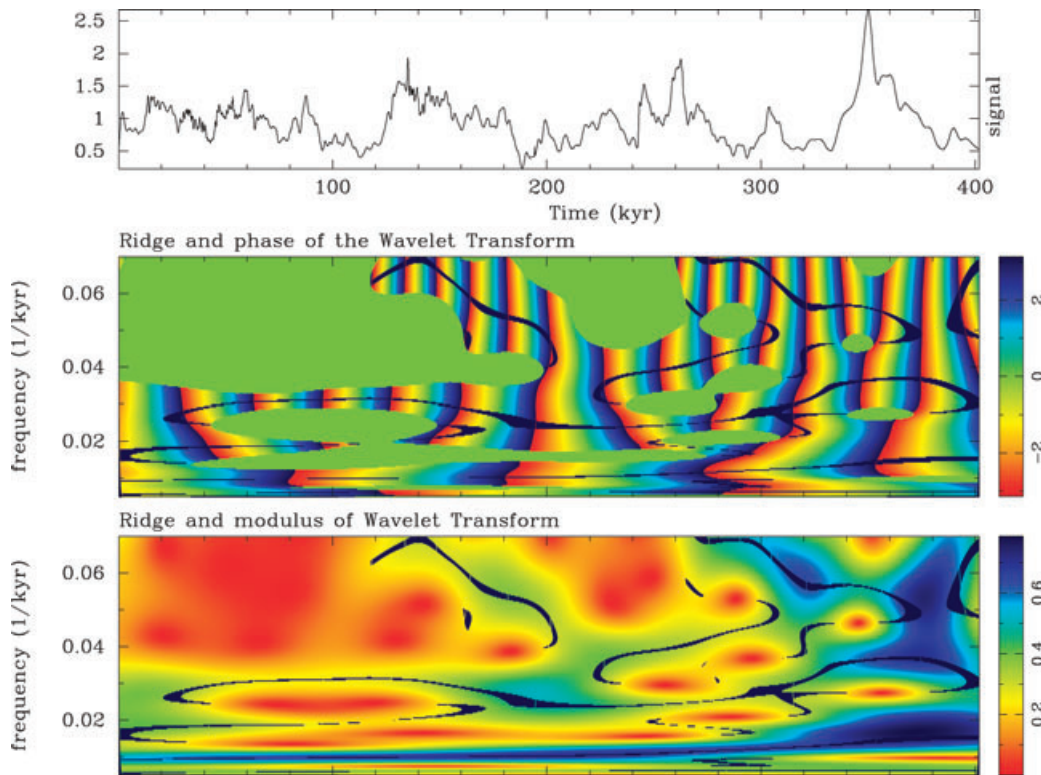


Figure 11. Top: relative palaeointensity of proxy record sampled on Portuguese margin over the last 400 kyr. Middle: phase of the CCWT with orbital frequencies extracted (superimposed black lines): continuous and slightly modulated ridge (eccentricity) and discontinuous ridges for precession and obliquity. Bottom: modulus of the CCWT.

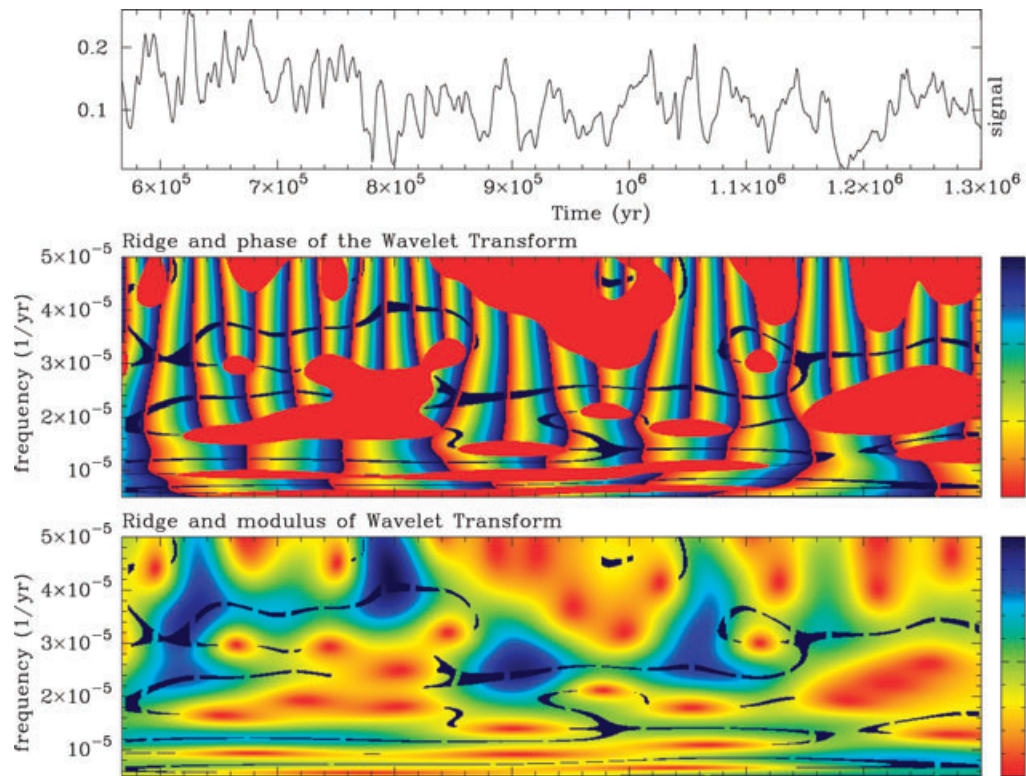


Figure 12. Top: relative palaeointensity of MD972140 (West Equatorial Pacific) between 570 and 1300 kyr. Middle: phase of the CCWT with orbital frequencies extracted (superimposed black lines). Continuous and modulated eccentricity ridge. Discontinuous obliquity ridge during the first 500 kyr. Bottom: modulus of the CCWT.

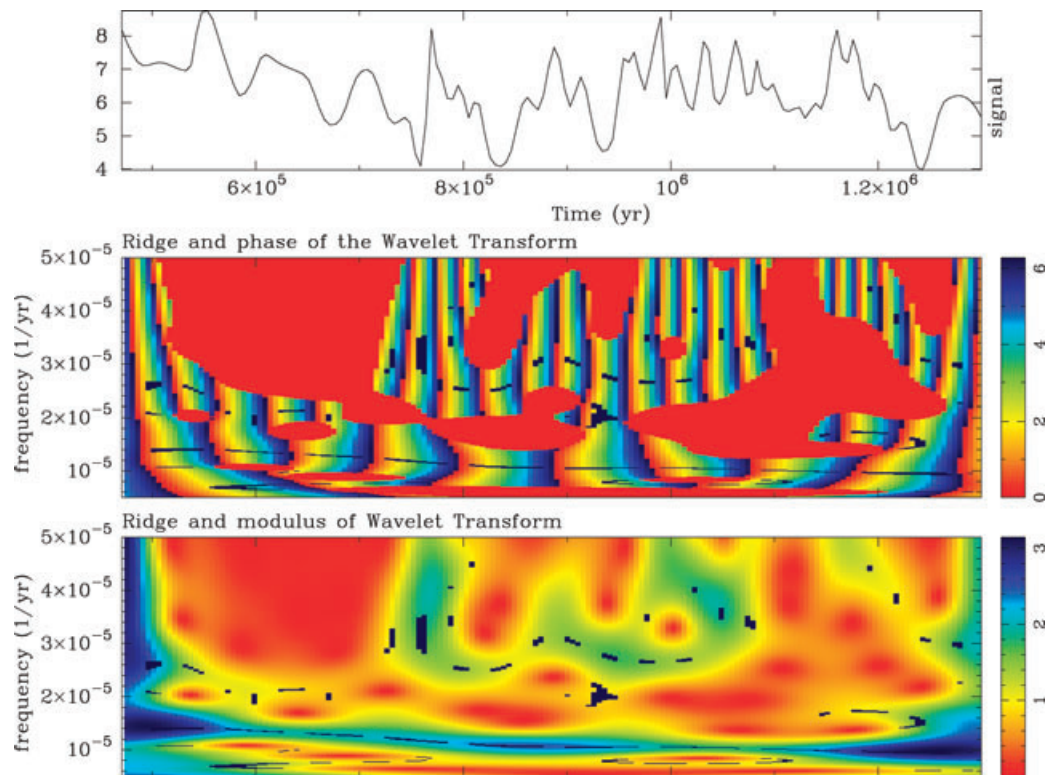


Figure 13. Top: authigenic $^{10}\text{Be}/^9\text{Be}$ ratio variations of MD972140 (West Equatorial Pacific) between 570 and 1300 kyr. Middle: phase of the CCWT with orbital frequencies extracted (superimposed black lines). Continuous and modulated eccentricity ridge. Obliquity ridge during the first 200 kyr BP. Bottom: modulus of the CCWT.

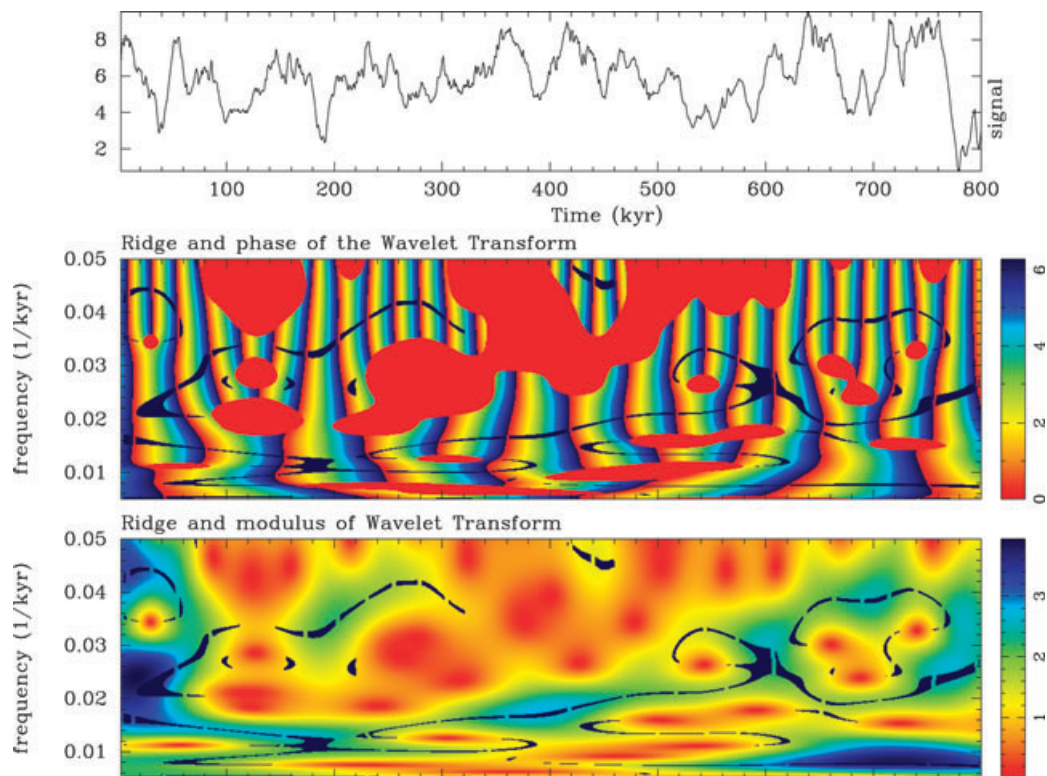


Figure 14. Top: Sint 800 curve, stack of marine relative palaeointensity records over the last 800 kyr. Middle: phase of the CCWT with orbital frequencies extracted (superimposed black lines). Eccentricity ridge during the last 400 kyr. Bottom: modulus of the CCWT.

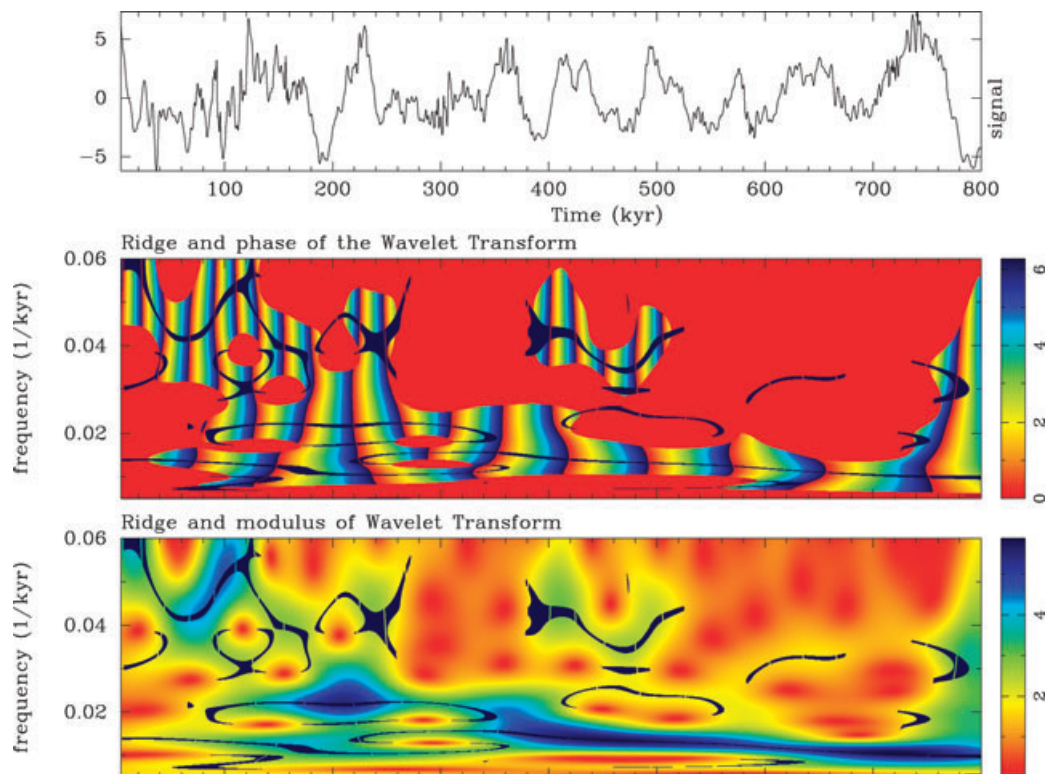


Figure 15. Top: magnetization of the deep seafloor over the last 800 kyr. Middle: phase of the CCWT with orbital frequencies extracted (superimposed black lines): modulated and shifted eccentricity ridge. Discontinuous obliquity ridge between [100 and 300] and [400–550] kyr BP. Precession ridge the first 100 kyr BP. Bottom: modulus of the CCWT.

Fig. 10 shows the time-scale analysis of the $\delta^{18}\text{O}$ record which represents the regime of the global ice volume changes over the last 800 kyr. The instantaneous frequency extracted from the phase corresponds to eccentricity (black superimposed line) around $0.0098 \text{ (kyr)}^{-1}$ ($T = 102 \text{ kyr}$) between 0 and 200 kyr BP, and they are progressively shifted to the frequency 0.014 (kyr)^{-1} ($T = 71.43 \text{ kyr}$) between 200 and 800 kyr BP. Two discontinuous ridges corresponding to obliquity component between $[0.21 \text{ and } 0.223] \text{ (kyr)}^{-1}$ (i.e. $T = [44.85\text{--}47.65] \text{ kyr}$) are extracted for the interval $[0\text{--}200] \text{ kyr BP}$ and between $[550 \text{ and } 600] \text{ kyr BP}$. There appears a third ridge in the frequency range of $[0.03\text{--}0.042] \text{ (kyr)}^{-1}$ between $[400 \text{ and } 460] \text{ kyr BP}$, that cannot be firmly identified.

Previous coupled reconstructions of palaeomagnetic and $^{10}\text{Be}/^9\text{Be}$ ratio (e.g. Carcaillet *et al.* 2003; Thouveny *et al.* 2004; Carcaillet *et al.* 2004a) have revealed their ability to accurately reconstruct the amplitudes and rhythms of dipole moment variations. For the Brunhes normal chron and the late Matuyama reversed chron, they confirm that geomagnetic excursions and polarity reversals occurred during geomagnetic dipole lows (Valet & Meynadier 1993; Valet *et al.* 2005) that induced cosmogenic nuclide overproductions due to pervasive penetration of galactic cosmic rays into the atmosphere (e.g. Carcaillet *et al.* 2004b). Such overproduction events are recorded in the ice cores of Greenland and Antarctica.

Fig. 11 is the result of analysis of the 400 kyr relative palaeointensity record of the Portuguese margin (Thouveny *et al.* 2004). We observe that the extraction of ridges provides a strong signal along the eccentricity component (black superimposed line) around approximate frequency $0.0098 \text{ (kyr)}^{-1}$ (i.e. 102 kyr) in the interval $0\text{--}270 \text{ kyr BP}$, then with a progressive frequency shifting to 0.016 (kyr)^{-1} ($T = 62.5 \text{ kyr}$) in the older part of the record. A continuous and modulated ridge appears around 0.025 kyr^{-1} in the interval $[180\text{--}300] \text{ kyr BP}$ corresponding to the obliquity component. This ridge is connected to a ridge around 0.03 (kyr)^{-1} in the interval $[20\text{--}180] \text{ kyr BP}$ and the last 100 kyr BP. This is due to the presence of interferences (specific loops ridge around minima of energy), between orbital components. Two discontinuous ridges are extracted in the frequency range of $[0.04\text{--}0.07] \text{ (kyr)}^{-1}$, in the intervals $[120\text{--}200]$ and $[280\text{--}380] \text{ kyr BP}$. They partially correspond to the precession component ($[0.042\text{--}0.052] \text{ (kyr)}^{-1}$) slightly shifted to high frequencies (see Figs 4 and 9).

An interesting case concerns the records of the MD972140 core sampled in West Equatorial Pacific which covers the interval $[500\text{--}1300 \text{ kyr}]$. Two proxy records were studied: the relative palaeointensity record, analysed in Fig. 12, and the past geomagnetic field activity record from cosmogenic isotope (the authigenic $^{10}\text{Be}/^9\text{Be}$ ratio; Carcaillet *et al.* 2003, 2004b), analysed in Fig. 13. In both cases, a discontinuous ridge is extracted around the obliquity, in the frequency range $[0.0232\text{--}0.0243] \text{ (kyr)}^{-1}$ ($T = 41\text{--}43 \text{ kyr}$), in the interval $[500\text{--}700] \text{ kyr BP}$. A continuous slightly modulated ridge, close to the first mode of eccentricity, is extracted in the frequency range $[0.0095\text{--}0.012] \text{ (kyr)}^{-1}$ ($T = [105.3\text{--}83.33] \text{ kyr}$) between $[500 \text{ and } 1200] \text{ kyr BP}$ (Fig. 12) and in the frequency range $[0.01\text{--}0.014] \text{ (kyr)}^{-1}$ ($T = [71.43\text{--}100] \text{ kyr}$) over the whole record (Fig. 13).

The last two analyses concerned the Sint 800 curve, stack of marine relative palaeointensity records (Guyodo & Valet 1999; Fig. 14), and the deep-seafloor palaeointensity anomaly record of the last 800 kyr, measured over the east flank of the southern East Pacific Rise (Gee *et al.* 2000; Fig. 15). The instantaneous frequency of eccentricity appears in both cases, in the last 400 kyr BP around $0.0098 \text{ (kyr)}^{-1}$ (102 kyr). During the first 400 kyr BP of the Sint

800 curve, some oscillations are present in frequency range of eccentricity ($[0.0098\text{--}0.012] \text{ (kyr)}^{-1}$; Fig. 14), while interference (loop in the ridge) between obliquity and eccentricity components is observed (Fig. 15) generating a shift of eccentricity component in the frequency range of $[0.0098\text{--}0.014] \text{ (kyr)}^{-1}$ for the deep-seafloor record. It is difficult to confirm clearly the existence of a single ridge of eccentricity in the first 400 kyr BP (Fig. 14). Fig. 15 presents two supplementary discontinuous ridges corresponding to the precession during the first 100 kyr BP, and obliquity component in the interval $[80\text{--}350] \text{ kyr BP}$.

All these time-series present frequency modulation laws or instantaneous frequencies in the interval $[0.008\text{--}0.033] \text{ (kyr)}^{-1}$ (i.e. $T = [30\text{--}125] \text{ kyr}$). The various origins and various recording mechanisms of these proxy records, as well as their similar frequency behaviour, suggest that they cannot be considered as all contaminated by palaeoenvironmental factors but represent accurate proxy records of the geomagnetic field variations. Therefore, the instantaneous frequencies, although discontinuously recorded and shifting in the range of orbital frequencies should be accepted as embedded in the long-term geomagnetic moment variation.

The 30–33 kyr period mostly present in the intervals $[0\text{--}200]$, $[500\text{--}700]$ and $[800\text{--}1100] \text{ kyr BP}$ lies between the pseudo-periods of the equinoctial precession ($\approx 17.2\text{--}23.8 \text{ kyr}$) and of those of obliquity ($\approx 38\text{--}42.5 \text{ kyr}$). This period might result from a resonance of the two beats since the obliquity cycle is approximately equal to 1.5 astronomical precession cycle. Alternatively, it could be a pseudo-harmonic of longer periods. The 40–50 kyr period mostly expressed in the long records might result from a bias of the obliquity period due to chronological errors. The range 80–120 kyr which encompasses characteristic periods of the eccentricity is well expressed in most time windows (Note that the pure eccentricity acts in the range of 83–125 kyr.) Finally, the range 67–80 kyr expressed in some windows of the long records might express mixtures of, or shifts between, the two framing period ranges, like ‘parasite frequencies’ (see Fig. 7).

5 CONCLUSIONS AND PERSPECTIVES

The existence of frequency modulation laws related to orbital frequencies (precession, obliquity and eccentricity) in the variations of the past geomagnetic field has been studied and highlighted, using the phase of the complex analysing wavelets. The instantaneous frequencies are extracted along ridges, trajectories corresponding to stationary phase points of the complex continuous wavelet transform. The interest of this method based on the phase and not on the modulus of wavelet coefficients is to extract frequency modulation laws even if the energy is low. Extraction of instantaneous frequencies is largely independent of the modulus, or of the energy of the signal.

Instantaneous frequencies of precession, obliquity and eccentricity (astronomical cycles) extracted from the phase of the wavelet transform of the insolation signal are in good agreement with the instantaneous frequencies extracted from the calculation of ‘pure’ astronomical parameters: the ridges are similar. Moreover, this method is robust in the presence of noise and does not need ‘*a priori*’ information on the signal. These analyses point out that the frequency behaviour of orbital components during the last 5 Myr does not present strong and continuous energies around the specific periods commonly accepted, that is, 21, 41, 100 and 400 kyr. They rather present eventual weak and/or discontinuous energies in ranges of frequency. A generalized application of such time-scale or

time-frequency methods would lead to a better understanding of the temporal evolution of Earth's orbit and of contributions of insolation variations to palaeoclimatic variations.

The different analyses of frequency modulation laws of palaeoproxy records of climate changes (oxygen isotope $\delta^{18}\text{O}$), of geomagnetic changes (relative palaeointensity, Sint 800 VDM, cosmogenic Beryllium ($^{10}\text{Be}/^9\text{Be}$) and the deep-seafloor magnetization record) all present instantaneous periods in the interval [30–125 kyr], particularly between 40 and 44 kyr for the obliquity, between 80 and 110 kyr, first mode of eccentricity, and in few cases between 20 and 23 kyr for the precession. They confirm the real presence of orbital frequencies in these palaeoproxy records. A comparison of phase diagrams of the CCWT of the VDM variations and glacial/interglacial variations near the 0.01 (kyr)^{-1} frequency revealed a clear similarity with a possible phase shift (Thouveny *et al.* 2008).

Consequently hypotheses of palaeoclimatic or orbital forcing via mechanical disturbances of the geodynamo cannot be rejected, particularly since the underlying mechanisms are now better physically constrained and understood.

ACKNOWLEDGMENTS

We thank particularly Alex Grossman for his constructive and fruitful discussions on the properties of the phase of the wavelet transforms. These studies were funded by the CNRS-INSU, Centre National de la Recherche Scientifique-Institut National des Sciences de l'Univers, Programs DyETI and SEDIT.

REFERENCES

- Bassinot, F.C., Labeyrie, L.D., Vincent, E., Quidelleur, X., Shackleton, N.J. & Lancelot, Y., 1994. The astronomical theory of climate and the age of the Brunhes-Matuyama magnetic reversal, *Earth planet. Sci. Lett.*, **126**(1–3), 91–108.
- Berger, A., 1977. Support for the astronomical theory of climate change, *Nature*, **268**, 44–45.
- Berger, A., 1988. Milankovitch theory and climate, *Rev. Geophys.*, **26**(4), 624–657.
- Berger, A. & Loutre, M.F., 1991. Insolation values for the climate of the last 10 million years, *Quatern. Sci. Rev.*, **10**, 297–317.
- Berger, A. & Loutre, M.F., 2004. Astronomical theory of paleoclimate, *Comptes Rendus Geosc.*, **336**(7–8), 701–709.
- Berger, A., Loutre, M.F. & Melice J.L., 1998. Instability of the astronomical periods from 1.5 Myr BP to 0.5 Myr AP, *Paleoclimates*, **2**(4), 239–280.
- Berger, A., Melice, J.L. & Loutre, M.F., 2005. On the origin of the 100-kyr cycles in the astronomical forcing, *Paleoceanography*, **20**(4), PA4019.
- Carcaillet, J., Bourles, D.L. & Thouveny, N., 2003. Geomagnetic moment instability between 0.6 and 1.3 Ma from cosmocnuclide evidence, *Geophys. Res. Lett.*, **30**(15), 1792, doi:10.1029/2003GL017550.
- Carcaillet, J., Bourles, D.L., Thouveny, N. & Arnold, M., 2004a. A high resolution authigenic $^{10}\text{Be}/^9\text{Be}$ record of geomagnetic moment variations over the last 300 ky from sedimentary cores of the Portuguese margin, *Earth planet. Sci. Lett.*, **219**(3–4), 397–412.
- Carcaillet, J., Bourles, D.L. & Thouveny, N., 2004b. Geomagnetic dipole moment and ^{10}Be production rate intercalibration from authigenic $^{10}\text{Be}/^9\text{Be}$ for the last 1.3 Ma, *Geochem. Geophys. Geosystem.*, **5**, Q05006, doi:10.1029/2003/GC000641.
- Carmona, R.A., Hwang, W.L. & Torresani, B., 1999. Multiridge detection and time-frequency reconstruction, *IEEE Trans. Sig. Process.*, **47**(2), 480–492.
- Channell, J.E.T., Hodell, D., McManus, J. & Lehman, B., 1998. Orbital modulation of the Earth's magnetic field intensity, *Nature*, **394**, 464–468.
- Christensen, U.R. & Tilgner, A., 2004. Power requirement of the geodynamo from ohmic losses in numerical and laboratory dynamos, *Nature*, **429**, 169–171.
- Copson, E.T., 1967. *Asymptotic Expansion*, The University Press, Cambridge
- Delprat, N., Escudie, B., Guillemain, P., Kronland-Martinet, R., Tchamitchian, P. & Torresani, B., 1991. Tech. Report, CPT-91, P. 2512, Luminy, Marseille, France.
- Erdélyi, A., 1956. *Asymptotic Expansions*, Dover Publications, Inc., New York.
- Fuller, M., 2006. Geomagnetic field intensity, excursions, reversals and the 41,000-yr obliquity signal, *Earth planet. Sci. Lett.*, **245**(3–4), 605–615.
- Gabor, D., 1946. Theory of communication, *J. Int. Elect. Eng. Lond.*, **93**, 429–441.
- Gee, J.S., Cande, S.C., Hildebrand, J.A., Donnelly, K. & Parker, R.L., 2000. Geomagnetic intensity variations over the past 780 kyr obtained from near-seafloor anomalies, *Nature*, **408**, 827–832.
- Grossmann, A., Holschneider, M., Kronland-Martinet, R. & Morlet, J., 1987. Detection of abrupt changes in sound signals with the help of wavelet transforms, *Adv. electron. electron phys.*, **Suppl. 19**, 289–306.
- Guillemain, P., Kronland-Martinet, R. & Martens, B., 1991. Estimation of spectral lines with the help of the wavelet transform: application in the NMR spectroscopy, in *Research Notes in Applied Mathematics: Wavelet and Applications*, pp. 48–60, ed. Meyer, Y., Masson-Springer-Verlag, Paris.
- Guillemain, P. & Kronland-Martinet, R., 1996. Characterization of acoustic signals through continuous linear time-frequency representations, *Proc. IEEE*, **84**(4), 561–585.
- Guyodo, Y., Gaillot, P. & Channell, J.E.T., 2000. Wavelet analysis of relative geomagnetic paleointensity at ODP Site 983, *Earth planet. Sci. Lett.*, **184**, 109–123.
- Guyodo, Y. & Valet, J.P., 1999. Global changes in intensity of the Earth's magnetic field during the past 800 kyr, *Nature*, **399**(6733), 249–252.
- Heslop, D., 2007. A wavelet investigation of possible orbital influences on past geomagnetic field intensity, *Geochem. Geophys. Geosys.*, **8**(3), Q03003, doi:10.1029/2006GC001498.
- Kent, D.V., 1982. Apparent correlation of paleomagnetic intensity and climatic records in deep-sea sediments, *Nature*, **299**, 538–539.
- Kronland-Martinet, R., 1989. Analysis, synthesis, and processing of audio signals: application of the wavelet transform, Doctorat d'Etat, Université Aix-Marseille II, Campus de Luminy, Marseille, France.
- Laskar, J., Joutel, F. & Boudin F., 1993. Orbital, precession and insolation quantities for the Earth from –20 myr to +10 myr, *Astron. Astrophys.*, **270**, 522–533.
- Malkus, W.V.R., 1968. Precession of the Earth's core as the cause of geomagnetism, *Science*, **160**(3825), 259–264.
- Melice, J.L., Coron, A. & Berger, A., 2001. Amplitude and frequency modulations of the Earth's obliquity for the last million years, *J. Clim.*, **14**(6), 1043–1054.
- Moreau, F., Gibert, D. & Saracco, G., 1996. Filtering non stationary in geophysic data with orthogonal wavelets, *Geophys. Res. Lett.*, **23**(4), 407–410.
- Papoulis, A., 1984. *Probability, random variables and stochastic processes*, McGraw-Hill, New York.
- Poincaré, H., 1910. Sur la précession des corps déformables, *Bull. Astron.*, **27**, 321–356.
- Saracco, G., 1989. Acoustic propagation through an inhomogenous medium in the case of harmonic and transient regime: asymptotic methods and wavelet transform, Thèse de Doctorat, Luminy, Université de la Méditerranée, Marseille, France, available at <http://tel.archives-ouvertes.fr/tel-00178676/fr/>.
- Saracco, G., 1994. Propagation of transient waves through a stratified fluid medium: wavelet analysis of a nonasymptotic decomposition of the propagator, *J. acoust. Soc. Am.*, **95**(3), 1191–1205.
- Saracco, G., Gazahnes, C., Sageloli, J. & Sessarego, J.P., 1990a. Time-scale analysis of acoustic scattering of elastic spherical shells from impulse sources, *J. Acoust.*, **3**, 381–392, available at <https://hal.archives-ouvertes.fr/hal-00018902>.

- Saracco, G., Guillemain, P. & Kronland-Martinet, R., 1990b. Characterization of elastic shells by the use of the wavelet transform, *IEEE Ultrasonics Symp.*, **2**, 881–885, available at <https://hal.archives-ouvertes.fr/hal-00177246>.
- Saracco, G., Sessarego, J.P., Sageloli, J., Guillemain, P. & Kronland-Martinet, R., 1991. Extraction of modulation laws of elastic shells by the use of the wavelet transform, in *Research Notes in Applied Mathematics: Wavelet and Applications*, pp. 61–68, ed. Meyer, Y., Masson-Springer-Verlag, Paris, available at <https://hal.archives-ouvertes.fr/hal-00157768>.
- Saracco, G., Labazuy, P. & Moreau, F., 2004. Localization of self-potential sources in volcano-electric effect with complex continuous wavelet transform and electrical tomography methods for an active volcano, *Geophys. Res. Lett.*, **31**, L12610.1-5, doi:10.1029/2004GL019554.
- Saracco, G., Moreau, F., Mathe, P.E., Hermitte, D. & Michel, J.M., 2007. Multi-scale tomography of buried magnetic structures. Its use in the localization and characterization of archeological structures, *Geophys. J. Int.*, **171**(1), 87–103.
- Thouveny, N., Carcaillet, J., Moreno, E., Leduc, G. & Nerini, D., 2004. Geomagnetic moment variation and paleomagnetic excursions since 400 kyr BP: a stacked record from sedimentary sequences of the Portuguese margin, *Earth planet. Sci. Lett.*, **219**(3–4), 377–396.
- Thouveny, N., Bourles, D., Saracco G., Carcaillet, J. & Bassinot, F., 2008. Paleoclimatic context of geomagnetic dipole lows and excursions in the Brunhes, clue for an orbital influence on the geodynamo?, *Earth planet. Sci. Lett.*, doi:10.1016/j.epsl.2008.08.020, **275**(3–4), 269–284.
- Tilgner A., 2005. *Precession driven dynamos*, (ABS), 10th Scientific Assembly IAGA.
- Valero, H.P. & Saracco, G., 2005. 3D Seismic endoscopy: multi-scale analysis and dynamic azimuthal filtering of borehole waves, *Geophys. J. Int.*, **161**, 313–328.
- Valet, J.P. & Meynadier, L., 1993. Geomagnetic-field intensity and reversals during the past 4 Million years, *Nature*, **366**(6452), 234–238.
- Valet, J.P., Meynadier, L. & Guyodo, Y., 2005. Geomagnetic dipole strength and reversal rate over the past two million years, *Nature*, **435**(7043), 802–805.
- Vanyo, J.P., 1991. A geodynamo powered by luni-solar precession, *Geophys. Astrophys. Fluid Dyn.*, **59**(1–4), 209–234.
- Vanyo, J.P. & Dunn, J.R., 2001. Core precession flow, structure and energy, *Geophys. J. Int.*, **142**, 409–425.
- Wu, C.C. & Roberts, P.H., 2008. A precessionally-driven dynamo in a plane layer, *Geophys. Astrophys. Fluid Dyn.*, **102**(1), 1–19.
- Xuan, C. & Channell, J.E.T., 2008. Origin of orbital periods in the sedimentary relative paleointensity records, *Phys. Earth Planet. Inter.*, **169**(1–4), 140–151.
- Yamazaki, T. & Oda, H., 2002. Orbital influence on Earth's magnetic field: 100,000-year periodicity in inclination, *Science*, **295**, 2435–2438.
- Yokoyama, Y. & Yamazaki, T., 2000. Geomagnetic paleointensity variation with a 100 kyr quasi-period, *Earth planet. Sci. Lett.*, **181**, 7–14.